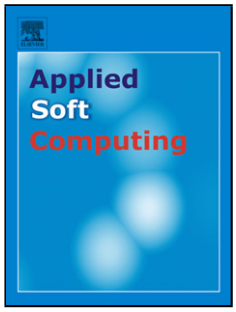

Title: An Integrated Approach for Head Gesture Based Interface

Authors: Gin Chong Lee, Chu Kiong Loo, Letchumanan Chockalingam

PII: S1568-4946(11)00456-X
DOI: doi:10.1016/j.asoc.2011.11.014
Reference: ASOC 1389

To appear in: *Applied Soft Computing*

Received date: 28-11-2010
Revised date: 16-8-2011
Accepted date: 9-11-2011

Please cite this article as: G.C. Lee, C.K. Loo, L. Chockalingam, An Integrated Approach for Head Gesture Based Interface, *Applied Soft Computing Journal* (2010), doi:10.1016/j.asoc.2011.11.014

(ASOC 1389)

Highlights

- This paper presents an original integrated approach to a head gesture based interface (HGI) which can perform both identity verification and facial pose estimation.
- Identity verification is performed by two-factor face authentication which is implemented by the combination of Topographic Independent Component Analysis (TICA) and Multispace Random Projection (MRP).
- Modified Synergetic Computer with Melting (Modified SC-MELT) is introduced to classify facial poses. Motion Profile Generator (MPG) is thoroughly developed during the integration to convert each estimated facial pose sequence into motion control signal to actuate motor movements.

An Integrated Approach for Head Gesture Based Interface

Gin Chong Lee [a,*], Chu Kiong Loo [b], Letchumanan Chockalingam [c]
[a] Faculty of Engineering and Technology, Multimedia University, Melaka, Malaysia
[b] Faculty of Computer Science and Information Technology, University of Malaya, Kuala Lumpur, Malaysia
[c] Faculty of Information Science and Technology, Multimedia University, Melaka, Malaysia

[*]Corresponding author at: Faculty of Engineering and Technology, Multimedia University, Jalan Ayer Keroh Lama, 75450 Melaka, Malaysia.

E-mail addresses: gclee@mmu.edu.my (G. C. Lee), ckloo.um@um.edu.my (C. K. Loo), chockalingam@mmu.edu.my (L. Chockalingam).

Abstract

The head pose and movement of a user is closely related with his/her intention and thought, recognition of such information could be useful to develop a natural and sensitive user-wheelchair interface. This paper presents an original integrated approach to a head gesture based interface (HGI) which can perform both identity verification and facial pose estimation. Identity verification is performed by two-factor face authentication which is implemented by the combination of Topographic Independent Component Analysis (TICA) and Multispace Random Projection (MRP). Modified Synergetic Computer with Melting (Modified SC-MELT) is introduced to classify facial poses. Motion Profile Generator (MPG) is thoroughly developed during the integration to convert each estimated facial pose sequence into motion control signal to actuate motor movements. The HGI is intended to be deployed as a user-wheelchair interface for disabled and elderly users in which only users with genuine face and valid token may be granted authorized access and hence pilot an Electric Powered Wheelchair (EPW) using their faces. The integration has been verified under a number of experiments to justify the feasibility and performance of the proposed face-based control strategy.

Keywords - facial pose estimation; face authentication; head gesture based interface; state machine; electric powered wheelchair.

1. Introduction

Recent evolution of Electric Powered Wheelchairs (EPWs) towards the trend of increasing intelligent has been encouraged by low cost processors and sensors. Various research efforts have been carried out in the last 10 years to develop more intelligent EPWs. Some of the existing EPWs are CALL Smart Wheelchair [1], Wheesley [2], OMNI [3], TAO projects [4], Rolland [5], MAid [6], NavChair [7], UPenn Smart Wheelchair [8], and SIAMO [9]. The main performance of EPWs can be generally classified into two major issues:

1) Autonomous and Safe Navigation Capabilities. Sensors such as laser range sensor, ultrasonic range detector, motor encoder, infrared proximity sensor and limit switch are embedded into controller system of wheelchair. Embedded sensors can help wheelchairs to localize their own position. Moreover, the wheelchair can travel to a predefined destination in an obstacle-free environment by performing

obstacle detection and avoidance autonomously. This research aims to offer safety, flexibility and mobility for wheelchair navigation [4][6][8][10][11][12][13].

2) User-wheelchair Interface. User-wheelchair interface aims to connect user's mind to the wheelchair actuator. User gives commands to wheelchair via interface and hence specifies the designated direction to move. Voice recognition, head gesture recognition and biosignal classification are often employed throughout implementing the interface [8][13][14][15] to offer easy operate, intuitive and low cost piloting for wheelchair [16].

This paper, however, will focus on the interface aspect of EPWs. As the head pose and movement of a user is closely related with his/her intention and thought, recognition of such information could be useful to develop a natural and sensitive user-wheelchair interface [17]. Moreover, we intend our interface to be used by severe disabled people who are only managed to move their heads and have difficulty to use joystick, chin stick and voice or breathe sensor assistive device. Head Gesture Based Interface (HGI) [13] may be one of the most suitable interfaces.

Typical Head Gesture Based Interface (HGI) is essentially a vision-based user-wheelchair interface that integrates approaches such as face detection, face tracking and head gesture recognition. Several research groups have already considered and deployed HGI in their EPWs. [13][17][18][19]. The HGI keeps users away from wearing any devices or have any devices attached to body parts which may diminish the uncomfortable feeling. However, these typical HGI systems do not take into account the privacy and identity security of the users, especially in real environment and remote monitoring of patient, identity steal and privacy invasion may occur which does not provide identity security to HGI-based wheelchair users. Improvements are necessary to include identity authentication in this interface.

We believe that an integrated approach to face authentication and facial pose estimation is one of the solutions in addressing the mentioned issue. In this paper, we intend to develop an HGI such that only authorized user is granted an access to pilot an electrical wheelchair. HGI first verify the identity of the user whether is genuine user or impostor via facial image acquired from camera and a valid token. Upon authentication, HGI recognizes commands given by user's facial poses based on images captured and generates the resulting motions as well as change of direction of the electrical wheelchair.

The rest of the paper is organized as follows: Section 2 presents the overview of HGI. Section 3 presents software implementation of the HGI (face authentication, facial pose estimation and motion profile generator (MPG)) which grants authorized access to valid user and provides control strategy for wheelchair navigation. Section 4 presents hardware configuration of the HGI deployed on wheelchair motion control. Section 5 shows the experimental results and discussions. Concluding remarks are drawn in Section 6.

2. Overview of Head Gesture Based Interface (HGI)

The present HGI was essentially developed such that the authorized access to the wheelchair can only be granted via a genuine face biometric and a valid PseudoRandom Number (PRN) token [20] prior to control the wheelchair freely. The system first attempts to keep track and capture user's face. Both PRN token and user's face biometric are sent for authentication mechanism. Via authentication mechanism, HGI limits the number of EPW users and so reduces the training size for facial pose estimation. It yields a user-dependent facial pose estimator which may, up to certain extent, have better classification accuracy. If the user's identity is authenticated successfully, facial pose estimation module will be activated and hence, images acquired from capturing device will be diverted to this module. Facial pose estimation module performs head gesture analysis and then generates the corresponding

motion control signals. However, unsuccessful authentication will block the access to wheelchair and request the user to repeat acquisition process.

The proposed HGI consists of two main implementations: software implementation and hardware implementation. In software implementation, acquired facial images were preprocessed to a fixed size and a face authentication module was developed to verify identity of a user whether or not a genuine user or an impostor. In addition, a facial pose estimation module was developed to classify facial pose images and generate the respective motion signals to actuate the desired movements on EPW. Meanwhile, hardware implementation aims to serve a physical platform for the deployment of software implementation of HGI.

3. Software Implementation

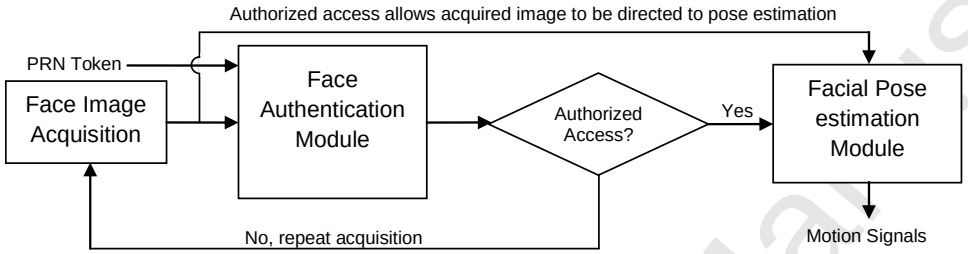

Fig. 1. Block diagram of the software implementation of HGI.

Fig. 1 depicts an overview framework of the HGI software implementation. It shows the facial image processing flow which comprises three stages: face image acquisition, face authentication module and facial pose estimation module.

Face image acquisition first captures facial image and performs necessary preprocessing to ensure user face is always within the region of image and accordingly cropped to a fixed size. It aims to overcome variance issues on illumination, scaling, translation, and in-plane rotation. Consequently, face authentication module which performs a two-factor based identity authentication in which a PRN token and a preprocessed facial image are received to determine whether or not to grant an authorized access. Unsuccessful authentication will request reacquisition of facial image and a valid token.

On the other hand, succeeded access will invoke and hence direct the acquired facial image to next stage, the facial pose estimation module. It consists of the required mechanisms for classifying a facial pose and generates the desired motion signals.

3.1 Face image acquisition

Face image acquisition intends to perform geometrical normalisation, illumination normalisation, and size each facial image into same dimension prior to the authentication and pose estimation stages. The module starts with eye detection [21] to locate the positions of both left eye and right eye on the acquired image. Using these positions, the distance between both eyes is determined.

In geometrical normalization wise, both left and right eyes are first aligned based on the distance line between both eyes such that it is parallel to a reference horizontal axis. This process may normalise in-plane rotation of facial image [22]. Each image is then scaled to a fixed size according to the distance between both eyes. Finally, each image is cropped to obtain the face region and Retinex [23] is then applied for illumination normalization. Fig. 2 shows some exemplary images in face image acquisition.

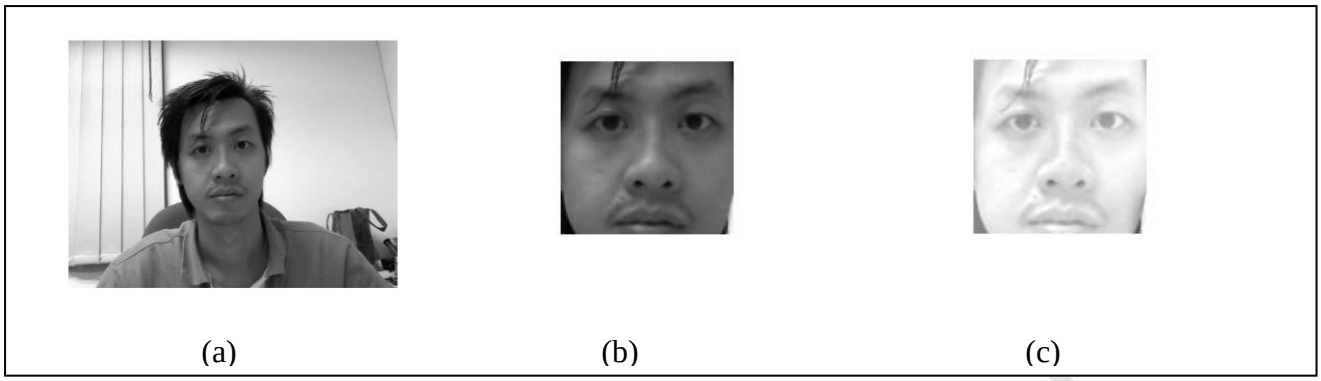

Fig. 2. Facial image pre-processing results: a) Captured image b) Geometrical normalised image c) Illumination normalised image.

3.2 Face Authentication Module

Upon the image acquisition, normalized facial data and a PRN token are forwarded to face authentication module which consists of main algorithms, namely TICA (Topographic Independent Component Analysis) [24] and MRP (Multispace Random Projection) [20]. TICA model works as feature extractor in conjunction with the implementation of MRP to provide a more secure and trustable two-factor face authentication system.

Two-factor face authentication is distinct from single-factor face authentication in the sense that, in the later, the system knows the identity of a user in advance, by means of physical tokens, but only face data is used to verify whether the a priori user is a client or an impostor; while in two-factor face authentication, in addition to the system knows the identity of a user in advance, both facial data and tokens will be used in authentication process. As depicted in Fig. 3, after images are acquired, it is followed by four crucial mechanisms: feature extraction, MRP, template matching and decision making.

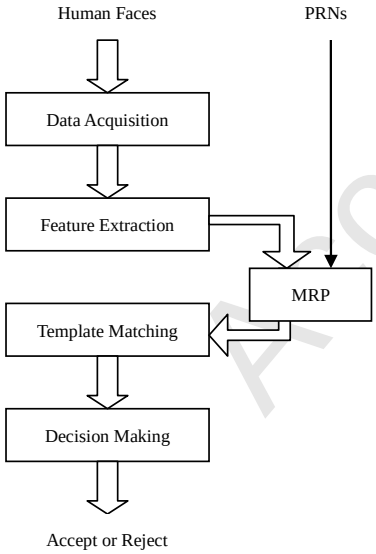

Fig. 3. Two-factor face authentication system.

3.2.1 Topographic Independent Component Analysis (TICA)

Feature extraction generally plays important role to condense the original face data. Working in original high-dimensional data space has been shown in [25] to be not efficient. Redundant information in original data might, up to certain extent, deteriorate the performance of face authentication. Therefore, the extraction of relevant, discriminant features from the original data is necessitated. Subsequent authentication processes are performed in the reduced dimension feature subspace. Fastidious preference of the features is crucial in face authentication. Subspace analysis is one of the most important and well-known approaches to implement feature extraction. PCA is one of the pioneer subspace analysis methods often used for face recognition [26] [27] and face authentication [28]. Another is based on LDA as in [25]. While, in [29], ICA has been claimed to offer improved success rate compared to equivalent system using PCA in face authentication.

In this section, we implement TICA to learn a set of topographically ordered basis vectors, namely the face subspace. TICA is one of the variants of classic ICA proposed by Hyvärinen and Hoyer [24]. In ICA face authentication [29], face subspace is obtained from manual ordering of the source vectors. With the aid of neighborhood enforcement in TICA, ordering of basis vectors can be done effortlessly by setting the appropriate dimension and mode ("torus" or "standard") of neighborhood matrix. In a similar way as in classic ICA [30], TICA factorises observed data x as a linear transformation of r basis function B and combining coefficients s:

$$x = Bs \tag{1}$$

where $B = \{b_1,\ldots, b_r\}$ is invertible and $s = \{s_1,\ldots, s_r\}$. Components s_i are assumed to be non-Gaussian and mutually independent in classic ICA. However, this assumption of independence has been relaxed in TICA. In other words, components that are close to each other within the scope of dependency defined by a neighborhood system as in [31] are assumed to be dependent; that is they are correlated in their energies within topography. Basic properties of TICA include:

1) All the components s_i are uncorrelated.

2) Components s_i that are far from each other are independent, at least approximately.

3) Components s_i that are near to each other tend to be active (non-zero) simultaneously, i.e. energies are positively correlated.

TICA is defined using a likelihood function with the introduction of neighborhood function h(i,j) [24]. Given m observed data $x(t)$, t=1,…, m, the log-likelihood function is estimated as

$$\log p(x \mid w) = \sum_{t=1}^{m}\sum_{j=1}^{r} G\Big(\sum_{i=1}^{r} h(i,j) < w_i, x(t) >^2\Big) + m \log |\det w| \tag{2}$$

where $w = B^{-1}$ is the inverse filter and the scalar function G has a similar role as the log density function of the independent component s_i in classic ICA. Learning algorithm of TICA model can be achieved by maximizing (2) with respect to w which can be implemented using gradient descent algorithm as in [32]. Having the learned TICA model, a gallery of face images will then be compressed by projecting them onto the face subspace in order to obtain the fixed length features vectors or "templates". During authentication, TICA model is applied as a feature extractor to compress a query face image to a fixed length feature vector with length n. Feature vector represents the mixing coefficients in (1) which can be used to reconstruct the face image by taking the product of feature vector with B.

Unfortunately, TICA subspace basis vectors are reversible or allow reconstruction of original image. By knowing the coefficient of a face in TICA model, the original face image can be simply reconstructed with considerable low error. It poses an enormous security hole for intruder to attack authentication system with a single factor (stolen face biometrics). Moreover, a large scale of facial

images acquisition and storage of facial data are necessary in face authentication; which might stem serious security concerns in terms of identity theft and privacy invasion. Furthermore, due to the vital permanence of face data, if a face is compromised, it is compromised forever. Non-revocation poses typical face authentication system stumbles upon the durable intrusion due to its single factor basis authentication. For this reason, the notion of cancellable biometric [20] [33] [34] has been proposed to formulate multifactor authentication. One of the promising formulations is Multispace Random Projections (MRP) [20].

3.2.2 Multispace Random Projections (MRP)

Multispace Random Projections (MRP) is a two-factor cancellable formulation which reinforces the security level of the system by necessitating a valid user-specific pseudorandom number (PRN) token and a genuine biometrics data for a permissible access. MRP consists of feature extraction and multispace random projections. In feature extraction stage, raw facial biometrics datum is transformed into a fixed length feature vector $x \in \Re^n$ via a TICA feature extractor. In multispace random projection phase, the feature vector is further projected onto a sequence of random spaces that were derived from a PRN token. A set of unique random projection (RP) vectors is formulated as follows to include G users to generate G different RP features, i.e., multiple random subspaces R^k:

$$v^k = \sqrt{(1/m)} R^k x \tag{3}$$

where $R \in \Re^{mn}$ is a m x n random matrix, $m \leq n$, n is the feature length and $k=1,\ldots,G$ .. The mixing process is revocable but non-reversible which makes replacing biometrics as simple as replacing PRNs [20]. During authentication, feature vector is mixed with the legitimate PRN token to result random projection vector for template matching.

3.2.3 Template Matching and Decision Making

Consequently upon MRP, template matching is performed on the random projection vectors based on Synergetic Neural Network (SNN) [35]. Dissimilarity score, s is computed according to the dot product between a query face q and SNN template face v_k^+ as in (4). The lower the score is, the more similarity between them.

$$s = 1 - v_k^+ . q \tag{4}$$

Lastly, binary decisions (reject or accept) will be determined based on the comparison, as in (5), between the dissimilarity score with a preset threshold value, t, which is conceptually similar as Uniform Threshold (UT) method [36]. The selection of suitable threshold value will be further addressed in section 5.1.1.

$$\text{If } s \leq t \text{ accept, otherwise reject} \tag{5}$$

During the authentication process, PRN tokens are particularly used to locate the claimed client template in database as well as to generate the user-specific random space and query face image is the input data to be projected onto TICA model and MRP space for identity verification.

3.3 Facial Pose Estimation Module

Following a succeeded authentication, facial pose estimation module is invoked. This module consists of two components – facial pose estimation and motion profile generator (MPG). We

implemented Modified SC-MELT algorithm [37] with learning interval of 2□ in facial pose estimation which the primary component in this module. We have classified the facial poses into 5 groups, accordingly, only LR, SR, F, SL, LL easy motions (detailed in section 5.2). We named this motion range as safety range. It is due to the fact that the disabled is having limited range of visual field about the environment. Moreover, adjustment of the speed is disabled during the piloting. These limitations are actually playing critical role to avoid any unexpected accident to occur. Motion Profile Generator (MPG) is the secondary component which converts the results of pose estimation to motion control signals required to actuate EPW motors movements.

Since the implementation is towards the application of head gesture based interface for wheelchair control, several assumptions have been made in this pose estimation model. The system only operates on and needs to estimate the pose only for the person or a group of persons on which it has been trained. The head is only allowed to rotate around one axis. Pose variation is restricted to a range that contains all of the facial features information seen from a frontal view.

3.3.1 Modified SC-MELT

In this section, we implement Modified SC-MELT algorithm [37] in the context of view-based facial pose estimation [38]. It is the primary component in facial pose estimation module. This facial pose estimation consists of two main stages: learning of adjoint prototypes and classification of facial images. The learning stage provides a group of view-based adjoint prototypes which is kept in synergetic memory for future classification task. In second stage, classification of a query image is performed based on the values of order parameter computed from the projection result on each view-based adjoint prototype.

Adjoint prototype learning could be treated as supervised learning of synergetic memory cells. The system assumes that label of view information is known for each learning images. It starts by acquiring learning images. Facial poses that fall under a predefined range of view angles will be gathered into prototype pattern clusters. In other words, one view-based adjoint prototype is learned by using the learning images from that prototype pattern cluster only.

In Modified SC-MELT, this is achieved implicitly by the matrix *E*. Hence, number of learning images in a prototype pattern cluster and number of prototype pattern clusters must be incorporated into the dimension of matrix *E* according to (6) and (7).

$$V_p^+ = E(V^T V + \rho_1 O + \rho_2 I)^{-1} V^T \tag{6}$$

E is enhanced identity matrix which is evaluated as:

$$E = \begin{pmatrix} e_1^{m(1)} & e_0^{m(2)} & \cdots & e_0^{m(M)} \\ e_0^{m(1)} & e_1^{m(2)} & \cdots & e_0^{m(M)} \\ \vdots & \vdots & \ddots & e_0^{m(M)} \\ e_0^{m(1)} & e_0^{m(2)} & \cdots & e_1^{m(M)} \end{pmatrix} \tag{7}$$

where entries of matrix *E* is defined as line vector of dimension *j*:

$$e_0^j = (0,...,0) \tag{8}$$

$$e_1^j = (1,...,1) \tag{9}$$

and V_p^+ denoted the adjoint prototype matrix with penalty terms, *O* is a unity square matrix and *I* is an identity matrix. By this adaption, it enhances the learning performance and offers flexibility to govern

the level of "melting", where both $\rho 1$ and $\rho 2$ are free parameters to adjust the level of melting and hence classification rate. The assumptions made in original SC-MELT [39] are still obeyed in the Modified SC-MELT. The selection of the optimal values for $\rho 1$ and $\rho 2$ in our context of application is similar to MPOD [40].

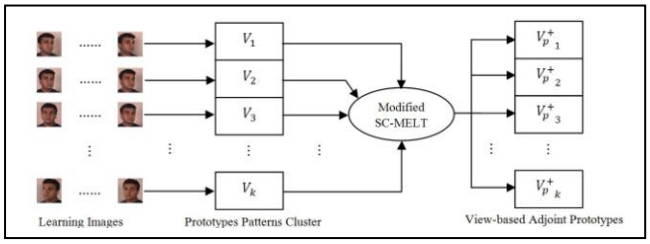

Fig. 4. Adjoint prototypes learning for pose estimation.

As depicted in Fig. 4, *k* individual facial pose clusters are taken into account. All learning prototypes fall into the same range of view angle are grouped into a common prototype matrix V_k. Modified SC-MELT algorithm then "melts" or combines all prototype images into each corresponding individual synergetic memory cell namely the adjoint prototype $V_{p\,k}^{+}$. The grouping of learning pose images in a facial view cluster is greatly dependent on the learning interval used. For instance, let us consider a learning interval is 2□, and then pose images with view angle -10□, -8□, -6□, -4□, -2□, 0□, 2□, 4□, 6□, 8□, and 10□ of each subject would be used to form the facial view cluster for FRONT poses. It is noted that only eleven images are used for each subject during the learning rather than a huge series of images grouped into the same pose cluster. In section 5.2, experiment demonstrates that it is sufficient to perform pose classification even only small number of images used for each cluster.

The computed view-based adjoint prototypes $V_{p\,k}^{+}$ serve as basis for pose estimation. An adjoint prototype corresponds to a synergetic memory cell that produces the maximum response for a specific class of pose stimuli. In this context, a synergetic memory is where facial images of certain view angles can reside in; a specific class of pose stimuli means facial images of specific view angles. The response of an input query image is defined as (10). Ideally, an input of a specific pose has maximum response to the adjoint prototype of the best matched pose cluster.

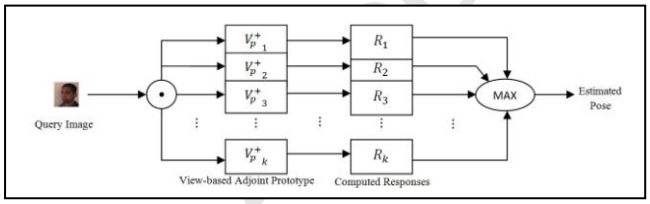

Fig. 5. Pose estimation based on maximum response (order parameter).

Applying the computed adjoint prototype matrix V_p^{+}, classification of a query image *q* can be achieved by using dot product of an adjoint prototype and query image to evaluate order parameter as follows:

$$\varepsilon_k = v_{p\,k}^{+} \cdot q \tag{10}$$

The pose estimation is performed by classifying a query facial pose image *q* into one of the facial pose clusters according to the notion of "winner takes all" (WTA) [41]. Query facial pose images mean

the images that are not used during the learning of adjoint prototypes. As illustrated in Fig. 5, a query facial pose image *q* is projected onto each adjoint prototype and the cell response defined by order parameter is then computed. This yields cell responses R_1, R_2, ... , and R_k . The query image q is classified using WTA criterion: it belongs to the ith pose cluster if cell response R_i is a maximum value.

3.3.2 Motion Profile Generator (MPG)

Motion Profile Generator (MPG) is the secondary component in facial pose estimation module. It in fact is a state machine which plays important role to convert the results of pose estimation to motion control signals required to actuate EPW motors movements. Fig. 6 illustrates input and output of the MPG.

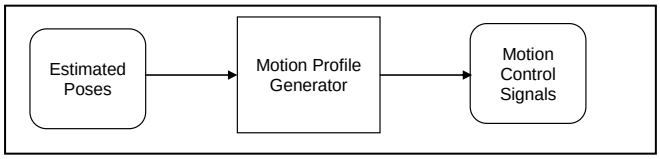

Fig. 6. Input and output of MPG.

In order to reduce the impact of undesired facial pose recognition errors on the control of the wheelchair, especially unwanted motions originate from user mistakes, MPG state machine is defined thoroughly. As depicted in Fig. 7, MPG orders the sequences of the facial pose input signal and generates the motion control signals to control the EPW accordingly. Menu selection begins at 'neutral' state. In 'neutral' state, both left and right motors remains at static mode which is stop condition. A sequence of motion control signals 'Right - Front' leads to select an option from the menu. The developed MPG offers two modes of operation: navigation mode and on-the-spot turn mode. A decision can be made by moving the head to the left. As long as a decision is made, a ready state, either 'ready to move' or 'ready to turn', will be followed. 'Front' signal initiates the next movement. Right and left motion control signals in Fig. 7 refer to small right or large right and small left or large left respectively.

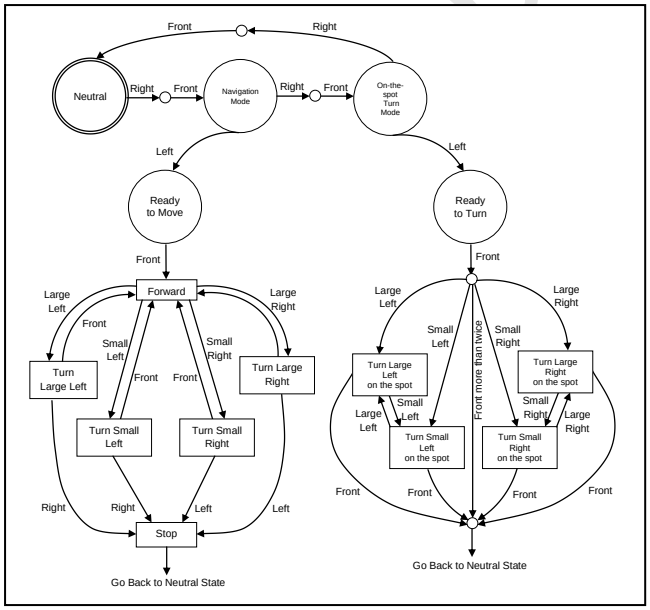

Fig. 7. State transition diagram used by MPG to pilot electrical wheelchair.

Navigation mode allows the user to pilot the wheelchair in order to travel freely around an environment. Available motor movements include forward, turn large left, turn small left, turn large right, and turn small right. It is noted that no backward movement is offered for safety reason. In this mode, front signal always leads to drive the wheelchair to move in forward direction. In order to stop the wheelchair, a pair of opposite motion control signals must be issued. For instance, 'large left-right', 'large right-left', 'small left-right', and 'small right-left' will lead the current state transition to 'stop' state which namely returns the transition to 'neutral' state.

On the other hand, on-the-spot turning mode allows the users change the orientation of the wheelchair. Available motor movements include 90□ turn right (large right), 45□ turn right (small right), 90□ turn left (large left), and 45□ turn left (small left). Once entered into this mode, only front signal can make current state transition to 'neutral' state. Motion control signals which are in the same direction will orientate the wheelchair in the same direction. For example, 'large left-small left' will swap the current state, turn large left on the spot, to next state, turn small left on the spot and vice versa. All motion profiles of the wheelchair are governed by the developed MPG based on the notion of state machine.

4. Hardware Implementation

Although software implementation of HGI is the main focus in this work, a prototype EPW, as shown in Fig.8, has been developed and merely used as a testing platform to examine the functionality of the HGI. It is a conventional wheelchair which has been modified with two motorized rear wheels using a pair of Vexta 100 gear ratio DC motors. These motors produce a low speed-high torque motion which is suitable to carry human weight on wheelchair. Moreover, gears are added on both the motor shaft and the wheel shafts and driven by belt. This setup provides flexibility for motor replacement in case of faulty motor situation.

Fig. 8. EPW Prototype for HGI deployment.

The hardware configuration of our EPW is depicted in Fig. 9 and compromises the following components:

1. Camera is used to capture the facial images of the user.
2. Upon image reception, central PC executes HGI software implementation, namely, face image acquisition, face authentication and facial pose estimation. Central PC contains the trained database used for authentication and pose estimation. Eventually, central PC generates and sends the motion control signals to the SBC.

3. PhidgetInterfaceKit1019 is a Single Board Computer (SBC) which offers a compact integration of hardware peripherals. It interconnects motion control signals to motor driver boards.

In general, HGI software implementation is deployed in central PC to provide an interface for user to pilot the EPW and SBC acts as a bridge in hardware implementation to obtain both real-time motion control signal sampling and high performance piloting control.

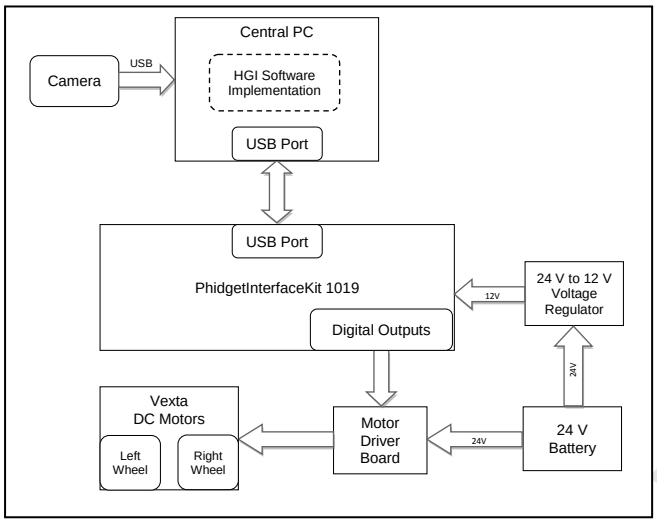

Fig. 9. Block diagram of EPW hardware configuration.

5. Experimental Results and Discussions

Several experiments were conducted to investigate the potential and feasibility of the integration of face authentication and facial pose estimation as HGI in practical environment. We have evaluated the HGI performance from two points of view. The first point of view was on individual performance of both identity authentication and facial pose estimation using benchmark datasets. Second point of view merely concentrates on the experiments to verify the feasibility of the developed HGI in EPW navigation.

5.1 Face Authentication

These experiments were conducted on frontal face images from the publicly available Face Recognition Technology (FERET) face database [42]. One face image for each 1000 persons was randomly chosen from dataset "fa" as training set. 500 clients and 500 impostors were selected from dataset "fb". Each client and impostor group were further grouped into 250 validation set and 250 test set. Validation set and testing set were chosen to be independent to present objectives results.

Each of the face images was preprocessed using eye finding, geometrical normalization and illumination normalization as described in section 3.1 and was sized into 35x35 pixels. The evaluations were performed for dimension of TICA subspace set at 100 and MRP at 100. Synergetic Neural Network (SNN) was adapted in decision making to compute the access scores between a query face and template face. Training set was used for TICA subspace learning. The validation set was selected to produce client and impostor access scores in order to evaluate system performance. Finally, the test set was used to simulate realistic authentication tests.

a) *Validation Set:* The performance measures of face authentication can be done by plotting the False Accept Rate (FAR hereinafter) versus the False Rejection Rate (FRR hereinafter) with threshold value being an implicit parameter. Different pairs of FAR and FRR values can be computed by selecting different values of threshold values. Such a plot is known as Receive Operating Characteristic (ROC hereinafter) Curve. It indicates the performance of an authentication system. ROC curve closer to axes implies better performance. Moreover, equal error rate (ERR hereinafter) occurs when FAR = FRR provides alternative approach to observe the system performance and hence determine threshold setting.

b) *Test Set:* To simulate realistic authentication performance, both FAR and FRR were determined using threshold value at ERR using test set.

5.1.1 Evaluation Results

We have implemented MRP cooperatively with TICA (TICAmrp hereinafter) which is two-factor authentication model and hence we evaluated the performance for both stolen face and stolen token scenarios. For comparison purpose, we have also implemented MRP cooperatively with PCA [43] (PCAmrp hereinafter) with same setup as TICAmrp.

The ERR for both stolen face scenario and stolen token scenario in TICAmrp is 0.064 and 0.076 respectively [Fig.10 (a) and 11 (a)]. PCAmrp exhibits higher EER for both stolen face scenario and stolen token scenario which is 0.068 and 0.088 respectively [Fig.10 (c) and 11 (c)]. In term of ROC curve, TICAmrp shows a closer curve to axes in both scenarios [Fig.10 (b) and 11 (b)] as compared to PCAmrp [Fig.10 (d) and 11 (d)]. Frequency distributions of scores measure for TICAmrp and PCAmrp are shown in Fig.12 (a) and 12 (b) respectively. In TICAmrp, genuine user scores distribute from 0.89 to 0.98, impostor scores for stolen token distribute from 0.935 to 0.99 and impostor scores for stolen face distribute from 0.945 to 0.985. PCAmrp exhibits comparative results similar as TICAmrp except that it has wider genuine user scores distributes from 0.89 to 0.985. The overlapping area between genuine distribution and impostor distribution is relatively smaller for both stolen token and stolen face scenarios in TICAmrp. TICAmrp and PCAmrp exhibits concentrative scores distribution in both genuine and impostor which might be due to the adaptation of MRP.

Table 1a summarises the results obtained on testing set. Threshold value at 0.9557 for TICAmrp and 0.9561 for PCAmrp is the average value obtained at EER for both stolen token and stolen face scenarios. It is noticeable that error rate of TICAmrp is considerable lower than PCAmrp which is in average about 7.8%.

Table 1a
Results from Test Set

Algorithm	Threshold	FAR	FRR	(FAR+FRR)/2
TICAmrp	0.9557	0.0880	0.0680	0.078
PCAmrp	0.9561	0.0900	0.0760	0.083

The experiment results imply that the performance of TICAmrp shows more reliable authentication result as compared to PCAmrp. In addition to include stronger security due to non-reversible property of MRP feature vector, results shows TICAmrp has high success rate in authentication. Original MRP provides the flexibility in controlling the mean and standard deviation of impostor distribution meanwhile maintain genuine distribution which can minimize the overlapping area, details is in [20]. In this work, SNN was adapted in score measure which might break the flexible control of impostor distribution. However, experiment results show that we have gained reliable

authentication performance. Moreover, best performance warrants TICAmrp to be applied for further application in HGI development.

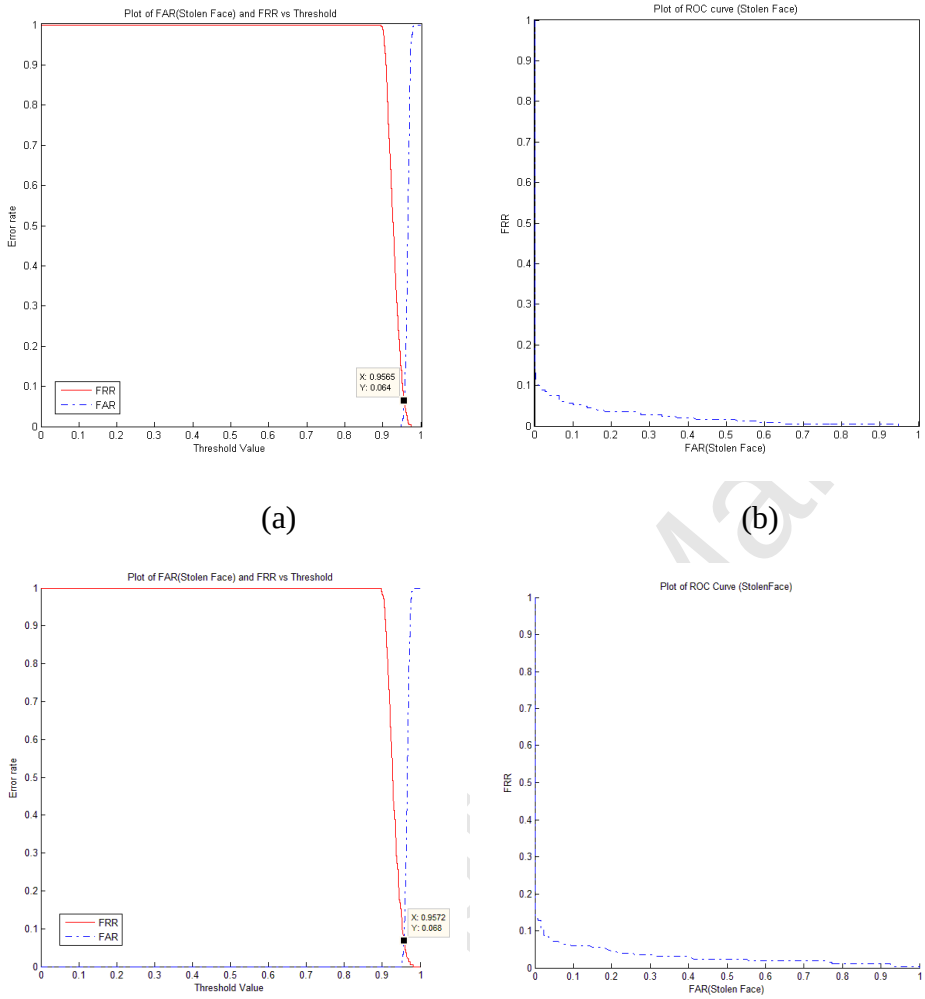

Fig. 10. Performance in Stolen Face Scenario - TICAmrp : (a) EER = 0.064 (b) ROC curve and PCAmrp: (c) EER = 0.068 (d) ROC curve.

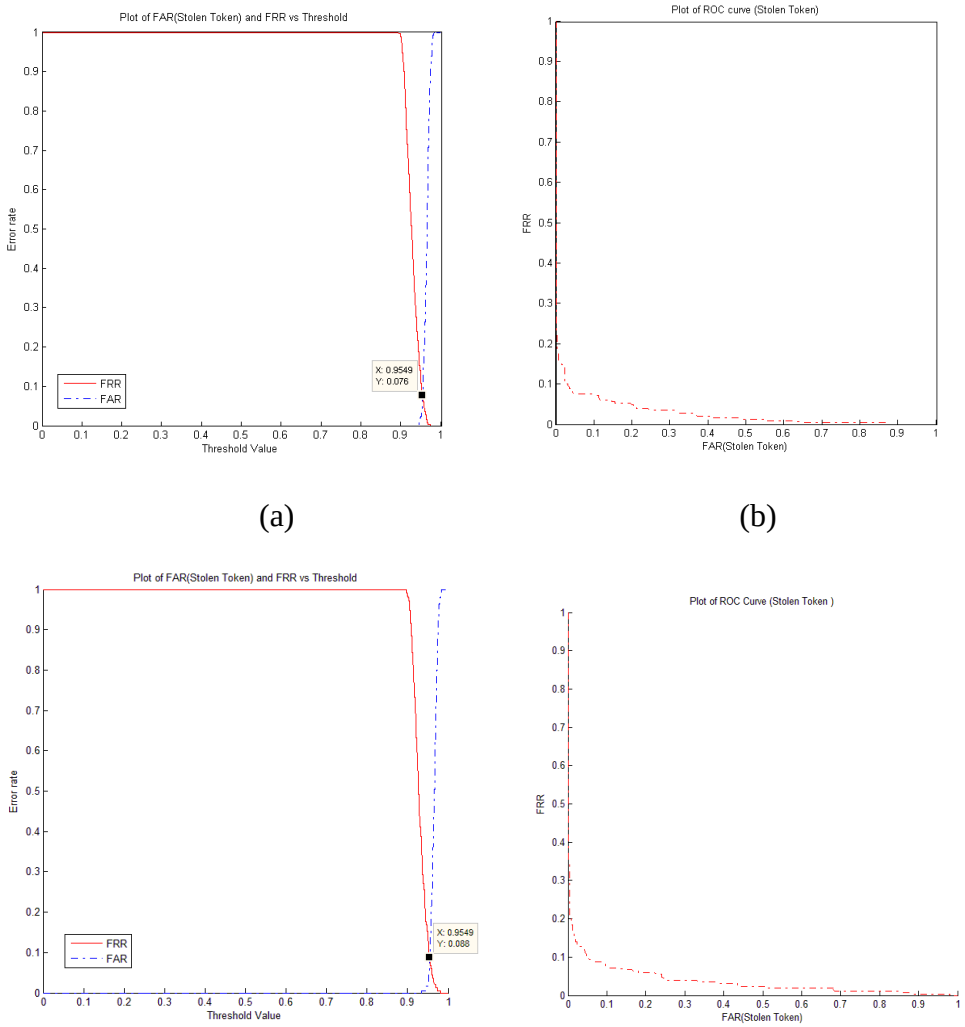

Fig. 11. Performance in Stolen Token Scenario – TICAmrp: (a) EER = 0.076 (b) ROC curve and PCAmrp: (c) EER = 0.088 (d) ROC curve.

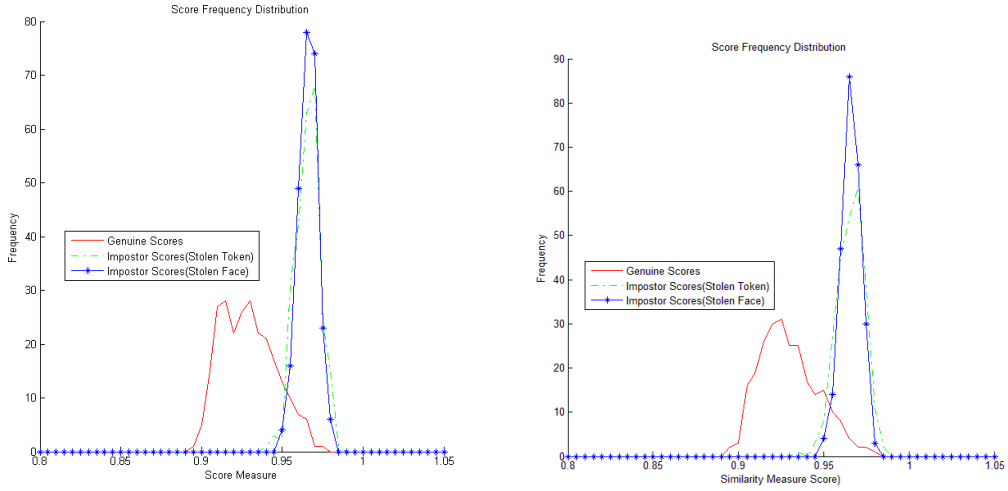

(a) (b)

Fig. 12. Frequency Distribution for Stolen Face Scenario and Stolen Token Scenario: a) TICAmrp and b) PCAmrp.

5.2 Facial Pose Estimation

In this section, we use a database of 10 subjects with 610 pose images retrieved from CUbiC FacePix(30) [44] for performance rating. The images have pan angles span from -30° to 30° with a consistent angle interval of 1°. In order to obtain objective experimental results, we divide the database into two independent sets, namely, training set and testing set. Training set is used for the learning of synergetic memory and testing set is the image set that is not used during training phase for classification evaluation. Each set is further divided into five pose clusters according to the specific pan angle range. In our field of problem, we define pose images spans from -30° to -21° as cluster LL (Large Left), pose images spans from -20° to -11° as cluster SL (Small Left), pose images spans from -10° to 10° as cluster F (Front), pose images spans from 11° to 20° as cluster SR (Small Right), and pose images spans from 21° to 30° as cluster LR (Large Right). Each face image is normalized and sized into 36 by 36 pixels in the experiment.

To assess the potential of SC-MELT based algorithms in pose estimation, two experiments were conducted for two different learning intervals used during the learning of synergetic memory, namely 2° and 5° . Learning intervals determine the number of images acquired for SC-MELT based algorithms to model each prototype pattern cluster by a synergetic memory cell. The evaluation begins to produce five view-based adjoint prototypes from training set. Then, we projected the query pose images taken from testing set to each synergetic memory cell and compute the corresponding order parameter, namely the response of query pose image in each synergetic memory cell. Thus, five cell responses are acquired for each query image. Based on the maximum cell responses for each query pose image, numbers of correctly classified images are determined to obtain the recognition rate. Experiment has been repeated for original SC-MELT as well as Modified SC-MELT for performance comparison.

5.2.1 Evaluation Results

Table 2a and table 2b show the classification rate of original SC-MELT and Modified SC-MELT for learning interval $2^{\square}$ and $5^{\square}$ respectively. Four significant observations can be identified from these tables. Firstly, Modified SC-MELT demonstrates better overall classification performance than original SC-MELT in both learning interval scenarios. Original SC-MELT shows overall performance which are 94.00% and 84.00% in $2^{\square}$ and $5^{\square}$ learning interval scenarios respectively. Modified SC-MELT manages to perform at classification rate of 96.00% and 88.25% respectively. Secondly, in both scenarios, original SC-MELT shows weaker rate in cluster SL and SR than Modified SC-MELT. It might be due to overfitting phenomenon. Thirdly, both algorithms perform better in the learning interval $2^{\square}$ scenario. This tells the potential of SC-MELT based algorithms in which adding more learning images might increase the accuracy. Lastly, for pose cluster F (front), Modified SC-MELT exhibits weaker performance.

It obviously shows that modification on original SC-MELT using penalty terms may increase the accuracy in facial pose estimation. In Modified SC-MELT, we sacrificed considerable low classification rate on FRONT cluster but we obtained higher classification rate on the profile view (LL, SL, SR and LR) clusters. Moreover, the flexibility on "melting level" control allows an adjustment which may be used to tune the classification rate. Some of the arbitrary examples of estimated pose images in the experiments are shown in Fig. 13.

In addition, classification results are also expressed as confusion matrices (c-matrices) and shown in Hinton diagram as depicted in Fig. 14 and Fig. 15. Each entry in a c-matrix denotes the number of pose images classified into *k*-th cluster [38]. The columns indicate predicted pose clusters and rows indicate the actual distribution of the poses under test. The right most column corresponds to LR-cluster and left most column corresponds to LL-cluster. The top row corresponds to the LL poses and bottom row corresponds to LR poses. The entries are expressed in term of percentage of classified poses and the size of each block in Hinton diagrams is proportional to the percentage values.

Hinton diagrams demonstrates that original SC-MELT and modified SC-MELT show consistent classification results in both learning interval scenarios. Pose images with similar view angle range tend to gather into the same cluster. There are gradual slopes off along the diagonal entries. In two extreme clusters namely cluster LL and LR, both original SC-MELT and Modified SC-MELT shows comparable results in both learning interval scenarios. Only small portions of test pose images were classified as adjacent cluster. However, in cluster F, Modified SC-MELT exhibits slightly weaker performance. It might be due to pose images in cluster F are intimately looked the same in which Modified SC-MELT could not distinguish them correctly. On the other hand, Modified SC-MELT exhibits better classification rate in cluster SL and SR for both learning interval scenarios. It is noticeable that original SC-MELT and Modified SC-MELT exhibit incorrect estimation only up to the adjacent clusters which demonstrates SC-MELT based algorithm is suitable to be implemented as facial pose classifier. Moreover, best performance warrants Modified SC-MELT to be applied for further application in HGI development.

Table 2a
Comparison of pose estimation between original SC-MELT and Modified SC-MELT (learning interval 2□)

Pose Clusters	Classification Rate (%)	
	Original SC-MELT	Modified SC-MELT
LL	94.00	94.00
SL	76.00	86.00
F	100.00	97.27
SR	80.00	88.00
LR	94.00	94.00
Overall	94.00	96.00

Table 2b
Comparison of pose estimation between original SC-MELT and Modified SC-MELT (learning interval 5□)

Pose Clusters	Classification Rate (%)	
	Original SC-MELT	Modified SC-MELT
LL	96.67	96.67
SL	71.67	91.67
F	85.00	83.75
SR	78.33	86.67
LR	86.67	90.00
Overall	84.00	88.25

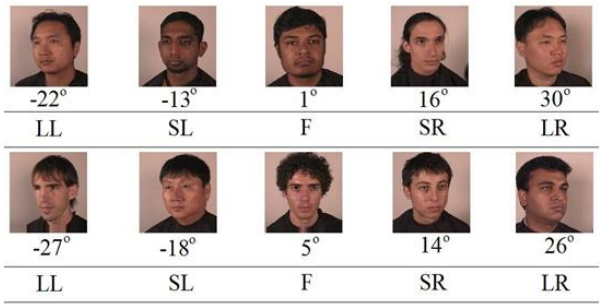

Fig. 13. Samples of estimated pose images from testing set.

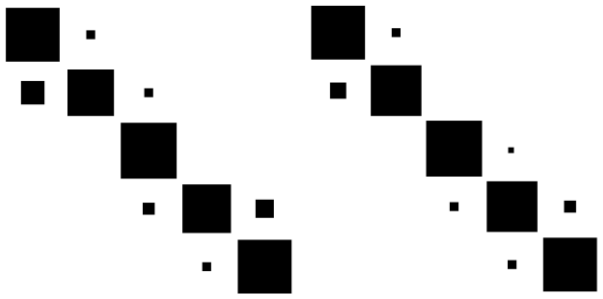

Fig. 14. Hinton diagrams show the accuracy of pose estimation on learning interval $2^{\square}$ for original SC-MELT (on the left) and Modified SC-MELT (on the right).

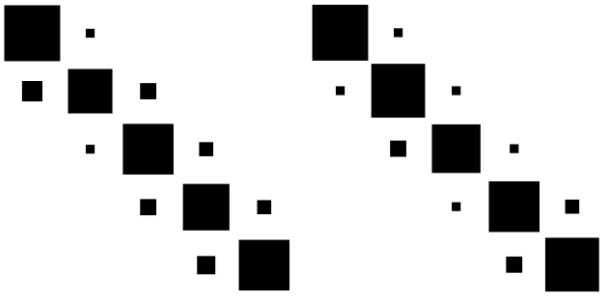

Fig.15. Hinton diagrams show the accuracy of pose estimation on learning interval $5^{\square}$ for original SC-MELT(on the left) and Modified SC-MELT (on the right).

Table 3
Computation times (time it took for order parameter calculation and classification) corresponding to the maximum classification accuracies obtained at learning interval $2^{\square}$

Computation Time (ms)	
Original SC-MELT	Modified SC-MELT
0.4939	0.8545

Computation times (Table 3) corresponding to maximum classification accuracy (learning interval $2^{\square}$) were evaluated for original SC-MELT and Modified SC-MELT. In this context, computation times refer to the average time taken to classify 50 query facial pose images. It obviously shows that adding penalty terms to original SC-MELT may increase the classification time in facial pose estimation. In Modified SC-MELT, we improved overall classification rate but it consumes 73% more classification time than original SC-MELT. However, in the application of HGI development, user may not be aware of significance of the delay in term of milliseconds.

5.3 Demonstration of EPW Navigation

In order to evaluate the proposed HGI, a Graphic User Interface (GUI) was developed which allows user to select the desired modes of control: hand control and HGI control. Hand control mode was simply used to generate a simple benchmark reference to be compared with HGI control mode. Via hand control mode, user controls the EPW using mouse-click on buttons to select the desired movements, include move forward, turn 45° to left, turn 90° to left, turn 45° to right and turn 90° to right. The GUI which allows user to select between hand control and HGI control is shown in Fig. 16.

Demonstrations of actual EPW navigation are presented here to show the feasibility of the developed HGI. We first adopted four basic motions to be tested as shown in Fig. 17 in an obstacle-free environment. The average time elapsed and number of moves in 5 trials for each basic motion made by hand control is shown in table 3a and those made by HGI control is shown in table 4b. Generally, results in table 4a shows time taken to issue the motion signals without any facial image processing involved. In average, about 2 seconds are required to execute a motion signal. Hence, we are able to determine the average speed of EPW from time taken to make forward 1.5 m motion. We have limited motor speed and tune it to produce average EPW speed at about 0.33 m/s which may be considered safe to carry human.

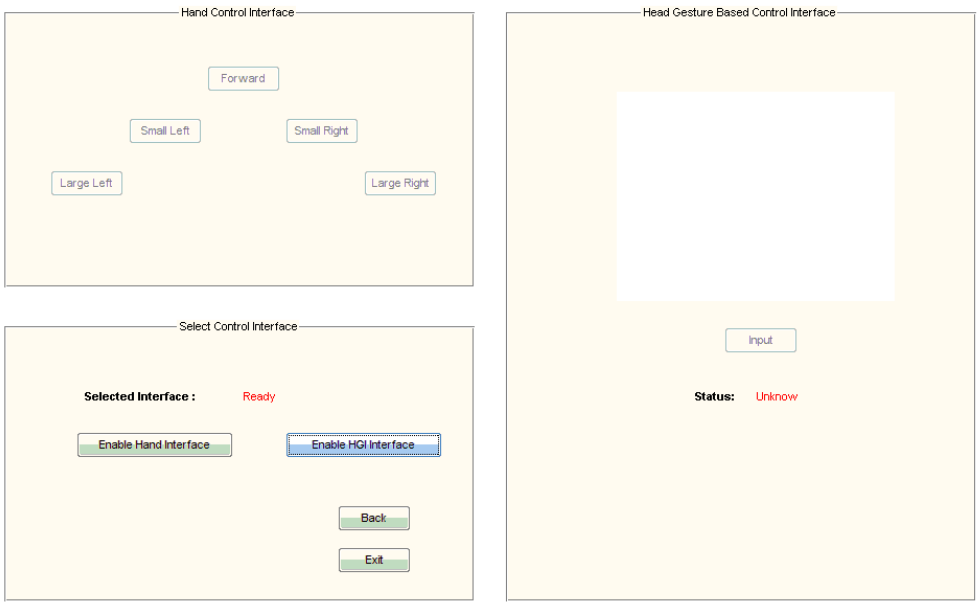

Fig. 16. Graphic User Interface (GUI) – Hand control and HGI control.

The results demonstrate that the developed HGI is able to pilot an EPW. All basic motions have been performed successfully. However, the EPW may not move in perfect straight-line path during forward motion. It may be due to the limitation of mechanical structure of the wheelchair: misalignment of left and right front-wheels and placement of the back-wheel motors is not evenly aligned at each side. Moreover, the disturbance on the floor surface during the experiment and unequal speed of left and right motors may also doubt the forward motion. It is also limited by the speed of the motor requires high precision calibration.

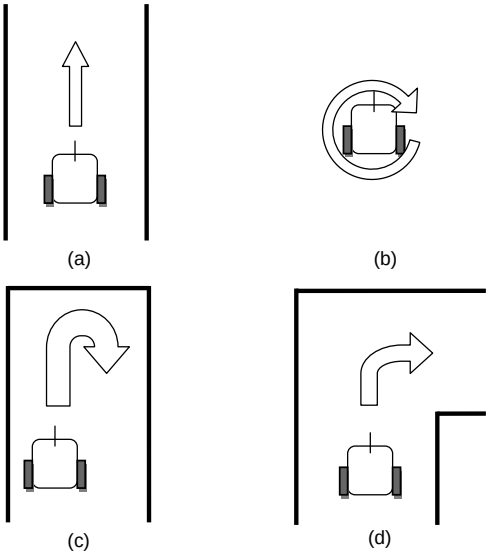

Fig. 17. Basic motions to pilot electrical wheelchair: (a) Forward (b) On-the-spot turn (c) U-turn (d) Corner turn.

Table 4a
Results of basic motions (Hand Control)

	Forward	On-the-spot turn		U-turn		Corner Turn	
	1.5m	CW	CC	Right	Left	Right	Left
Average time elapsed (s)	4.6	15.6	11.3	9.3	9.4	17.5	13.7
Average number of moves	2	7	6	5	5	7	7

Table 4b
Results of basic motions (HGI Control)

	Forward	On-the-spot turn		U-turn		Corner Turn	
	1.5m	CW	CC	Right	Left	Right	Left
Average time elapsed (s)	22.5	59.84	71.6	39.7	49.2	67.4	68.1
Average number of moves	2	6	7	4	5	7	7

It can be noted that average time taken by HGI control to make the same motion as compared to hand control is significant higher. HGI involves heavy facial processing in which each process consumes about 8 seconds before issue a motion signal.

Consequently, we have further applied the developed HGI to control the EPW in an indoor environment – a simple maze-type environment as depicted in Fig. 18. It shows the maneuverability of EPW when HGI is treated as the main piloting interface. For comparison purpose, time and number of moves taken to complete the task by hand control and HGI control have been recorded in Table 4c and Table 4d respectively.

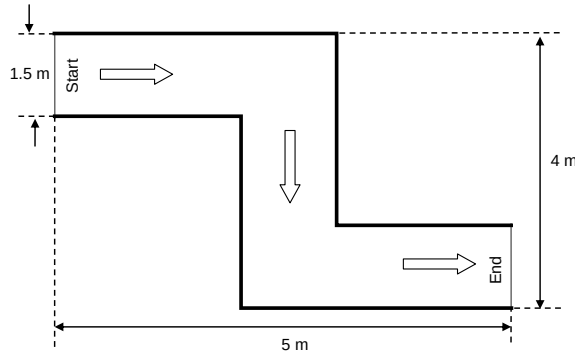

Fig. 18. A simple maze-type environment.

Table 4c
Results of simple maze-type motions (Hand control)

Trial	1	2	3	4	5
Time elapsed (s)	48	42.9	36.5	37.4	38
Number of moves	15	14	12	13	12

Table 4d
Results of simple maze-type motions (HGI control)

Trial	1	2	3	4	5
Time elapsed (s)	309.7	219.4	193	173.7	165.6
Number of crashes	2	1	0	1	0
Number of moves	22	15	14	14	13

Table 4c shows that hand control has completed the task successfully without getting crashed on any wall during the experiment. In first trial for both control modes, time taken and number of moves consumed are the highest. It is because user was not familiar about the environment. However, along the experiment further to subsequence trial, time and moves taken are considerable lower. Especially for HGI control (Table 4d), it can be noticed a gradually decrement on time elapsed to complete the same navigation. Fig. 19 presents a series of navigation sequences using HGI control: a) Start to travel in forward direction (Sequence 1 to 4); b) Turn right (Sequence 5 to 7); c) Travel in forward direction again (Sequence 8 to 10); d) Turn left (Sequence 11 to 15); e) Travel in forward direction and arrive at goal (Sequence 16).

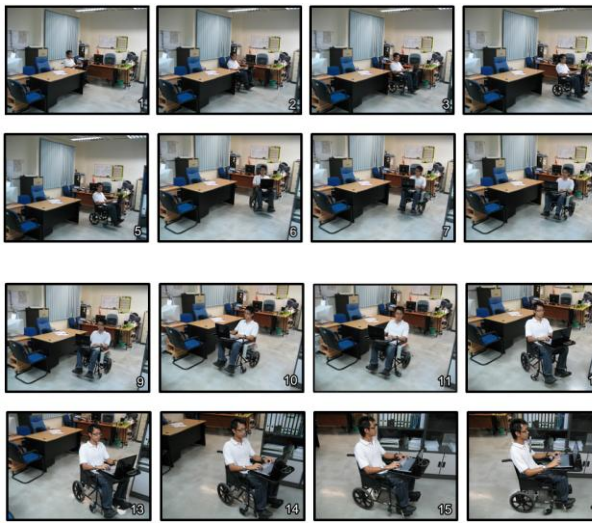

Fig. 19. A series of navigation sequences using HGI control in a simple maze-type environment.

Maximum payload which can be supported by the EPW is about 70kg yet, it is sufficient to support most of the users. It is limited by the mechanical structure and the material used to fabricate the wheelchair. Experiment results show that the developed MPG is working well and capable to generate the desired basic motions. However, the performance of HGI control is significantly lower than hand control in simple maze-type environment. It proves that the proposed HGI may be not appropriate to be used in an environment which requires additional and numerous control commands.

6. Concluding Remarks

As a conclusion, the integration of both identity authentication and facial pose estimation towards a HGI to pilot an EPW has been achieved. The contributions of the paper are the following: First, we have implemented and empirically evaluated the performance of TICA in conjunction with MRP to formulate two-factor face authentication as a step to improve the authentication system security. It has been employed to verify the identity of a user via a genuine face biometrics and a valid PRN token in EPW access. Secondly, we have implemented and empirically evaluated the performance of Modified SC-MELT in facial pose estimation. An MPG has been developed to capture the estimation results and hence generate the corresponding motion control signals for EPW navigation. Lastly, a case study has been conducted and clearly demonstrates the feasibility of the developed HGI in EPW navigation. We are confident that the HGI could be a practical solution for a user-wheelchair interface to pilot an EPW. Future research direction may focus on the enhancement to make this HGI system more “intelligent” in avoiding obstacles. Clinical test may be conducted on disabled users. Extensive experiment could be conducted to further investigate the potential of the HGI in piloting an EPW in environment with obstacle. Collision avoidance and wall follower may be considered to reduce the control burden on the user.

References

[1] CALL Centre, Learning through Smart Wheelchairs, University of Edinburgh, U. K., 1994.

[2] H.A. Yanco, A. Hazel, A. Peacock, S. Smith, H. Wintermute, Initial Report on Wheelesley: A Robotic Wheelchair system, Proceeding of Workshop on Developing AI application for the Disabled, International Joint Conference on Artificial Intelligence, Montreal, Canada, August 1995.
[3] H. Hoyer, U. Borgolte, Office Wheelchair with High Manoeuvrability and Navigational Intelligence for People with Severe Handicap, December 1996.
[4] T. Gomi, A. Griffith, Developing intelligent wheelchairs for the handicapped, Assistive Technology and Artificial Intelligence, Applications in Robotics, User Interfaces and Natural Language Processing, Lecture Notes In Computer Science, 1458:150-178, Springer-Verlag, Berlin, 1998.
[5] T. Röfer, A. Lankenau, Architecture and applications of the Bremen autonomous Wheelchair, in: Wang, P.P. (Ed.), Proceedings of the 4th Joint Conference on Information Systems, Vol. 1, Association for Intelligent Machinery, 1998, pp.365-368.
[6] E. Prassler, J. Scholz, M. Strobel, P. Fiorini, MAid: a robotic wheelchair operating in public environments, Lecture Notes In Computer Science, 1724:68-95, Springer-Verlag, Berlin, 1998.
[7] S.P. Levine, D.A. Bell, L.A. Jaros, R.C. Simpson, Y. Koren, J. Borenstein, The NavChair assistive wheelchair navigation system, IEEE Transcations on Rehabilitation Engineering, 7(4): 443-451, 1999.
[8] R.S. Rao, K. Conn, S. H. Jung, J. Katupitiya, T. Kientz, V. Kumar, J. Ostrowski, S. Patel, C. J. Taylor , Human robot interaction: application to smart Wheelchairs, Proceedings of IEEE International Conference on Robotics and Automation (ICRA 2002), 3583-3588, Washington, DC, USA, May, 2002.
[9] M. Mazo, J. C. Garcia, F. J. Rodriguez, J. Urena, J. L. Lazaro, F. Espinosa, Experiences in assisted mobility: the SIAMO project, Proceedings of IEEE International Conference on Control Applications, 2:766-771, September 2002.
[10] K. Schlling, H. Roth, R. Lieb, H. Stutzle, Improving the Quality of Life for the European Citizen, IOS Press, 331-335, 1998.
[11] A. C. Balcells, J. A. Gonz, TetraNauta: A Wheelchair Controller for Users with Very Severe Mobility Restriction, IOS Press, 336-340, 1998.
[12] G. Pires, U. Nunes, A wheelchair steered through voice commands and assisted a reactive fuzzy-logic controller, Journal of Intelligent and Robotic Systems, 43(3): 301-314, 2002.
[13] P. Jia, H. Hu, T. Lu, K. Yuan, Head gesture recognition for hands-free control of an intelligent wheelchair, Industrial Robot: An International Journal, 34(1):60–68,2007.
[14] K. H. Kim, H. K. Kim, J. S. Kim, W. Son, S. Y. Lee, A Biosignal-Based Human Interface Controlling a Power-Wheelchair for People with Motor Disabilities, ETRI Journal, 28(1):111-114, 2006.
[15] R.C. Simpson, S.P. Levine, Adaptive Shared Control of a Smart Wheelchair Operated by Voice control, Proceeding of IEEE/ RSJ International Conference on Intelligent Robots and Systems (IROS'97), 622-626, 1997.
[16] J.W. Min, K. Lee, S.C. Lim, D.S. Kwon , Human-Friendly Interfaces of Wheelchair Robotic System for Handicapped Persons, International Conference on Intelligent Robots and Systems, EPFL, Lausanne, Switserland, October 2002.
[17] Y. Matsumoto, T. Ino, T. Ogasawara, Development of Intelligent Wheelchair System with Face and Gaze Based Interface, IEEE International Workshop on Robot and Human Interactive Communication, 2001.
[18] Y. Adachi, Y. Kuno, N. Shimada, Y. Shirai, Intelligent wheelchair using visual information on human faces, Proceeding of International Conference on Intelligent Robots and Systems (IROS' 98), 1:354-359, 1998.
[19] I. Yoda, K. Sakaue, T. Inoue, Development of Head Gesture Interface for Electric Wheelchair, Proceedings of the 1st international convention on Rehabilitation engineering, 1:77-80, 2007.

[20] A. B. J. Teoh, C. T. Yuang, Cancelable biometrics realization with multispace random projections, IEEE Transaction on Systems, Man and Cybernetics – Part B: Cybernetics, 37(5):1096-1106.October 2007.
[21] I. Fasel, B. Fortenberry, J. R. Movellan, A generative framework for realtimeobject detection and classification. Computer Vision and Image Understanding, In Press.
[22] B. J. Shastri, M. D. Levine, Face recognition using localized features based on non-negative sparse coding, Machine Vision and Applications, 18 (2):107-122, April 2007.
[23] B. Funt, F. Ciurea, J. McCann, Retinex in Matlab, Proceeding of the IS&T/SID Eighth Color Imaging Conference: Color Science, Systems and Applications, 112-121, 2000.
[24] A. Hyvarinen, P. O. Hoyer, M. Inki, Topographic independent component analysis, Neural Computation, 13(7):1527–1558, 2001.
[25] P. N. Belhumeur, J. P. Hespanha, D. J. Kriegman, Eigenfaces vs. fisherfaces: recognition using class specific linear projection, IEEE Transaction on Pattern Analysis and Machine Intelligence, 19 (7):711-720, 1997.
[26] L. Sirovich, M. Kirby, Low-dimensional procedure for the characterization of human faces, Journal of the Optical Society of America A 4, 519–524, 1987.
[27] M. Kirby, L. Sirovich, Application of the Karhunen-Loéve procedure for the characterization of human faces, IEEE Transaction On Pattern Analysis and Machine Intelligence 12:103–108, 1990.
[28] M. Turk, A. Pentland, Eigenfaces for recognition, Journal Cognitive Neuroscience, 3(1): 72–86, 1991.
[29] C. Havran, L. Hupet, J. Czyz, J. Lee, L. Vandendorpe, M. Verleysen, Independent component analysis for face authentication, Proceeding Knowledge-Based Intelligent Information & Engineering Systems, 1207-1211, 2002.
[30] P. Comon, Independent component analysis – a new concept ?, Signal Processing, 36:287 – 314, 1994.
[31] T. Kohonen, Self-organizing maps, Information Sciences, Springer, Heidelberg, Second edition, 1997.
[32] A. Hyvarinen, P. O. Hoyer, Emergence of topography and complex cells properties from natural images using extensions of ica, In Advances in Neural Information Processing Systems, 12: 827–833, 2000.
[33] G. Davida , Y. Frankel, B. J. Matt, On enabling secure applications through off-line biometric identification, Proceeding of IEEE Symposium on Security and Privacy, 148, 1998.
[34] N. Ratha , J. Connell, R. M. Bolle, Enhancing security and privacy in biometrics-based authentication systems, IBM Syst. J., 40: 614, 2001.
[35] T. Zhao, L. H. Tang, H. H. S. Ip, F. Qi , On relevance feedback and similarity measure for image retrieval with synergetic neural nets, Neurocomputing, 51:105-124, April 2003.
[36] F. Yang, S. Shan, B. Ma, X. Chen, W. Gao, Using Score Normalization to Solve the Score Variation Problem in Face Authentication, Proceeding of IWBRS, 31-38, 2005.
[37] G. C. Lee, C. K. Loo, Facial Pose Estimation using Modified SC-MELT *Second World Congress on Nature and Biologically Inspired Computing*, 2010, In press.
[38] S. Li, X. Lv, H. Zhang, View-Based Clustering of Object Appearances Based on Independent Subspace Analysis, Proceeding of 8th IEEE International Conference on Computer Vision. Vancouver, Canada. 295-300, July, 2001.
[39] R. W. Frischholz, F. G. Bö bel, K. P. Spinler, Face Recognition with the Synergetic Computer, Proceeding of IEEE International Conference On Applied Synergetics and Synergetic Engineering, Erlangen, Germany. 1994

[40] F. Hirotaka, K. Yoshinobu, H. Ichiro, Optimum Engine Mounting Layout using MPOD, The Japan Society of Mechanical Engineers. C, 70(689): 54-62, 2004.
[41] J. Dongarra, Performance of Various Computers using Standard Linear Equations Software, Computer Science Department, University of Tennessee, April, 1994.
[42] P. Philips, H. Moon, P. Rauss, S. Rizvi, The FERET database and evaluatioan methodology for face recognition algorithms, in: Proc. IEEE Conference on Compiter Vision and Pattern Recognition, 137-143, 1997.
[43] M. Partridge, R. Calvo, Fast dimensionality reduction and Simple PCA, Intelligent Data Analysis, 2(3):292–298, 1997.
[44] G. Little, S. Krishna, J. Black, S. Panchanathan, A Methodology for Evaluating Robustness of Face Recognition Algorithm with respect to Variation in Pose Angle and Illumination Angle, Proceeding of IEEE International Conference Acoustics, Speech, and Signal Processing, 2:89-92, 2005.